Surface-plasmon polaritons on metal–dielectric nanocomposite films

Zhimin Shi,[1,*] Giovanni Piredda,[1,2] Andreas C. Liapis,[1] Mark A. Nelson,[3] Lukas Novotny,[1] and Robert W. Boyd[1]

[1]*The Institute of Optics, University of Rochester, Rochester, New York 14627, USA*
[2]*Present address, Department Chemie und Biochemie, Ludwig-Maximilians-Universität München, 81377 München, Germany*
[3]*Department of Physics, New Mexico State University, New Mexico 88003, USA*
[*]*Corresponding author: zshi@optics.rochester.edu*

Received August 12, 2009; accepted October 1, 2009;
posted October 20, 2009 (Doc. ID 115563); published November 11, 2009

We observe experimentally that the reflectances of metal–dielectric nanocomposite films in the Kretschmann configuration show different characteristics, depending on the metal fill fraction f, that fall into one of three distinct regimes. In the "metallic" regime, in which f is large, the film supports conventional surface-plasmon polaritons (SPPs), and one can tailor the properties of the SPPs by controlling the value of f. In the "dielectric" regime, in which f is small, the film does not support any surface modes. In the intermediate "lossy" regime, the nanocomposite film supports a SPP mode that is different from that of a "metallic" film. These results are explained by using an anisotropic effective medium model and mode analysis.

OCIS codes: 240.6680, 160.4236.

The ability to control the properties of a surface-plasmon polariton (SPP) [1], such as its propagation constant, dispersion relations, and spatial mode profile, can greatly improve its performance in various applications, such as sensing [2], localized excitations of transitions [3], short-distance communications [4], and nonlinear optics [5–7]. It has been shown that the properties of SPPs can be tailored by the use of artificially synthesized periodic or random metal–dielectric nanocomposite materials [8–10]. Yet most of these studies assume that the metal in the nanocomposite is interconnected. In this Letter, we investigate how the properties of SPPs supported by random nanocomposite films evolve as the metal fill fraction is varied. Specifically, we explore the transition from continuous metal films to semicontinuous films to isolated nanoislands.

We fabricated a large collection of gold–air nanocomposite films with gold fill fractions f ranging from 1 to approximately 0.3. All samples are approximately 30 nm thick. The pure gold films were fabricated by using electron-beam evaporation, the films with high values of f were fabricated by using sputter coating, and those with moderate values of f were fabricated by using the pulsed laser deposition method [11]. We measured the reflectances of these nanocomposite films as functions of the incidence angle in glass θ_{inc} in the Kretschmann configuration at the wavelength of 1550 nm (see Fig. 1). The measured reflectance is calibrated with that from a bare prism under the same conditions to exclude the influence of unrelated interfaces. Five representative reflectance curves are plotted in Fig. 2. Here, sample 1 is a pure gold film, and the value of the gold fill fraction f decreases from approximately 0.85 to 0.4 for samples 2–5.

From scanning or transmission electron microscopy (SEM or TEM) studies (see, e.g., the insets of Fig. 1), one sees that the size of the in-plane features of all the nanocomposite films is much smaller than the wavelength. Furthermore, there is very limited structural variation along the thickness dimension. Thus, we here describe the macroscopic optical property of the nanocomposite films in terms of an anisotropic effective dielectric permittivity tensor $\vec{\varepsilon}_{\mathrm{eff}} = \mathrm{diag}[\varepsilon_{\mathrm{eff},x}, \varepsilon_{\mathrm{eff},y}, \varepsilon_{\mathrm{eff},z}]$. Here, the two in-plane components are equal to each other, $\varepsilon_{\mathrm{eff},x} = \varepsilon_{\mathrm{eff},y}$, and can be described by using the effective medium approximation (EMA) [12–14] as

$$f\frac{\varepsilon_{\mathrm{m}} - \varepsilon_{\mathrm{eff},x}}{\varepsilon_{\mathrm{m}} + \varepsilon_{\mathrm{eff},x}} + (1-f)\frac{\varepsilon_{\mathrm{d}} - \varepsilon_{\mathrm{eff},x}}{\varepsilon_{\mathrm{d}} + \varepsilon_{\mathrm{eff},x}} = 0, \tag{1}$$

where ε_{d} and ε_{m} are the dielectric permittivities of the bulk dielectric and metal, respectively, and f is the gold fill fraction. The out-of-plane component, $\varepsilon_{\mathrm{eff},z}$, is given by $\varepsilon_{\mathrm{eff},z} = f\varepsilon_{\mathrm{m}} + (1-f)\varepsilon_{\mathrm{d}}$. Figure 3 shows the calculated $\varepsilon_{\mathrm{eff},x}$ and $\varepsilon_{\mathrm{eff},z}$ of an anisotropic gold–air nanocomposite as functions of f at the wavelength of 1550 nm. The dielectric permittivities for air and bulk gold are 1 and $-114+10.9i$ [15], respectively. One sees that $\varepsilon_{\mathrm{eff},x}$ as a function of f shows three distinct regimes: a "metallic" regime for approximately

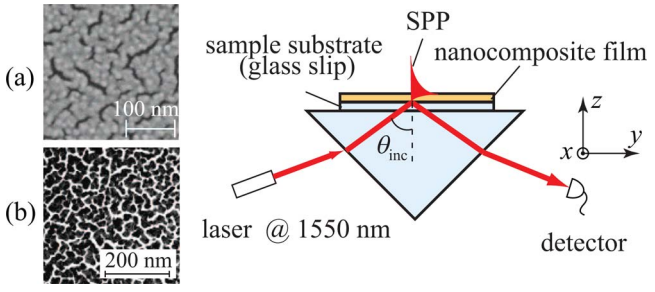

Fig. 1. (Color online) Schematic diagram of exciting SPPs using the Kretschmann configuration. Insets, (a) SEM and (b) TEM micrographs of two nanocomposite films with gold fill fraction $f \approx 0.85$ and $f \approx 0.65$, respectively.

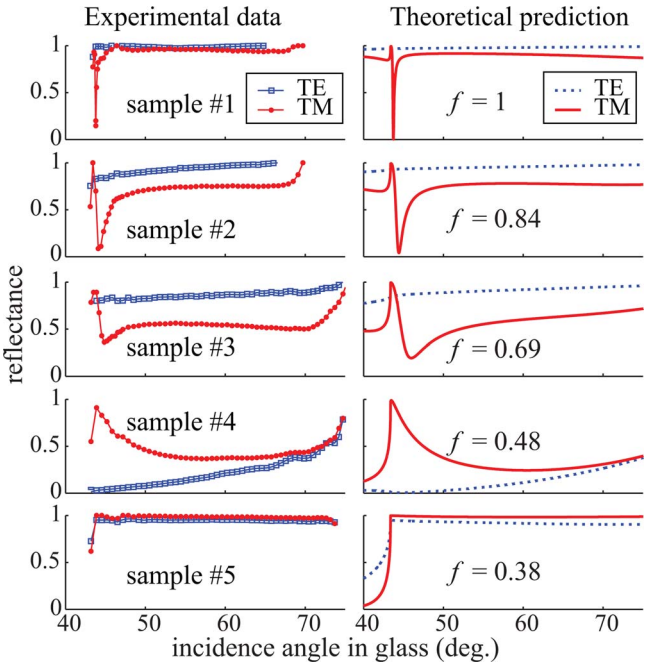

Fig. 2. (Color online) Measured (left) and calculated (right) reflectances of both polarizations in the Kretschmann configuration as functions of the incidence angle for five nanocomposite samples with decreasing gold fill fraction f.

$f>0.6$, a "dielectric" regime for approximately $f<0.4$, and a "lossy" regime for $0.4<f<0.6$. The prediction of the "lossy" regime by using the EMA model agrees with the experimental evidence that a semicontinuous nanocomposite film becomes highly lossy near its percolation threshold [16].

Using the above EMA model and the transfer matrix method, we calculate the reflectance from the five samples studied in Fig. 2. The fitted values of f agree reasonably well with the values obtained from the SEM or TEM micrographs of the samples. We account for the surface roughness of samples 2, 3, and 4 by assuming that the top 6 nm of the film, the thickness of which is consistent with the measurement by atomic force microscopy, to have a gold fill fraction of 0.5. One sees that the results of the calculation agree reasonably well with the experimental results, which demonstrates the qualitative validity of the EMA model [16,17]. With more knowledge about the geometry of the nanograins of the nanocomposite one could use more advanced effective medium theories [16,18,19] to calculate $\tilde{\varepsilon}_{\mathrm{eff}}$ more accurately.

To gain increased understanding of the results, we calculate the reflectance of a 30-nm-thick nanocomposite film as the value of f changes continuously from 1 to 0.3. As shown in Fig. 4, the reflectance for TM polarization as a function of θ_{inc} exhibits characteristics that fall into one of three distinct regimes, depending on the value of f. In the metallic regime, corresponding to $f>0.6$, the TM reflectance has a sharp narrow dip centered at some incidence angle larger than the critical angle (approximately 43.4°). As f decreases from unity, this dip broadens, while its center shifts toward larger incidence angles. These results indicate that both the real and the imaginary parts of the effective refractive index of the corresponding SPP mode increase as f becomes smaller. In the lossy regime, the reflectance for TM polarization has a peak shortly after θ_{inc} exceeds θ_c and then exhibits a very broad dip. As we show below, such a broad dip is related to the excitation of a SPP mode different from the one that can be excited on a conventional metallic film. In the dielectric regime ($f<0.4$), the reflectance becomes high for both polarizations for $\theta_{\mathrm{inc}}>\theta_c$, which indicates that the nanocomposite has the general property of a dielectric.

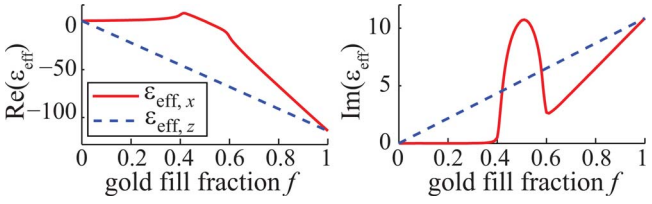

Fig. 3. (Color online) Calculated $\varepsilon_{\mathrm{eff},x}$ and $\varepsilon_{\mathrm{eff},z}$ of an anisotropic gold–air nanocomposite film at 1550 nm as functions of the gold fill fraction f.

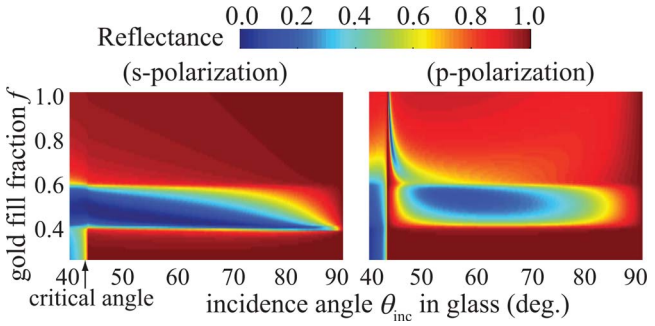

Fig. 4. (Color online) Calculated reflectances from a 30-nm-thick gold–air nanocomposite film, using the Kretschmann configuration as functions of the incidence angle θ_{inc} and the gold fill fraction f for (a) TE and (b) TM polarizations, respectively.

To illustrate how SPPs are excited on a lossy nanocomposite film, we plot in Fig. 5 the spatial field distribution of a Gaussian beam with FWHM of 5 μm at $z=0$ incident on three nanocomposite films with $f=0.6$, 0.55, 0.5. Here the two-dimensional calculation assumes that both the field and the film are uniform in the x direction. The values of θ_{inc} in the three cases are 49°, 57°, and 57°, respectively. For a nanocomposite film at the boundary between the metallic and the lossy regimes ($f=0.6$), a mode with field localized at the air–film interface is excited. As f decreases, this mode becomes excited less efficiently, while a second mode, with the field localized on the glass–film interface, is gradually excited. For $f=0.5$, the field distributions in the glass are almost identical for TE and TM polarizations. However, the field distribution within the film is very different, indicating the excitation of SPPs for TM polarization.

These results can be also understood by considering which modes of the glass–film–air geometry are excited when a plane wave is incident from glass onto a film with different values of the metal fill fraction. In general, there are four modes associated with such a geometry when the influence of leaky modes is in-

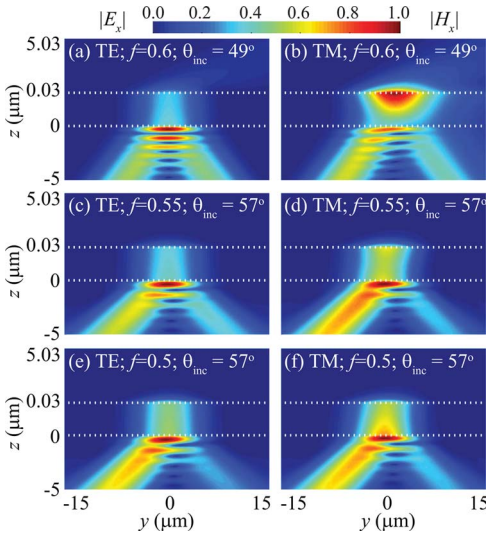

Fig. 5. (Color online) Spatial field amplitude ($|E_x|$ for TE and $|H_x|$ for TM polarization) distribution of a Gaussian beam of 5 μm FWHM incident on three nanocomposite films with different values of f. The film is expanded by a factor of 100 in the z direction for visual purposes.

cluded [20]. The complex effective refractive index n_{spp} of each mode is shown in Fig. 6. By calculating the interaction strength between each of these modes and an incident plane wave [20], we determine which modes are most strongly excited for each specific situation. For films in the metallic regime, modes 3 and 1 correspond to the sharp and shallow dips in the reflectance, respectively. The shift and broadening of the sharp dip as f decreases agree with the evolution of n_{spp} for mode 3. In the dielectric regime, modes 2 and 3 correspond to the two Brewster modes incident from glass and air, respectively. In the intermediate lossy regime, modes 3 and 4 correspond to the air–film and glass–film modes shown in Fig. 5, respectively.

In conclusion, we have studied the SPPs supported by a metal–dielectric nanocomposite film sandwiched between air and glass. We show both experimentally and theoretically that both "metallic" and "lossy" nanocomposite films can support SPPs and that the properties of the supported SPPs can be adjusted by controlling the metal fill fraction. However, the SPPs that can be excited on a continuous and a semicontinuous nanocomposite film using the Kretschmann configuration are actually different modes, and they have very different characteristics. Our analysis provides a design guideline for random metal–dielectric nanocomposite for different applications of SPPs.

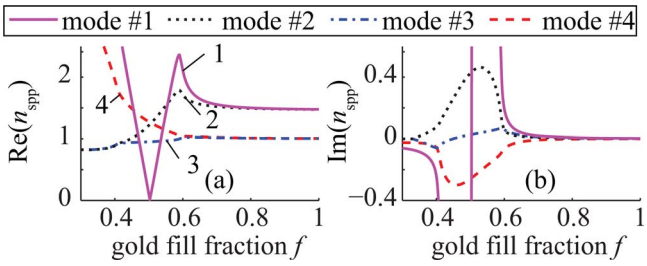

Fig. 6. (Color online) (a) Real and (b) imaginary parts of the effective refractive index of the supported SPP modes as functions of the gold fill fraction f.

The authors gratefully acknowledge the help of Brian McIntyre and Brad Deutsch in sample preparation and characterization. M. A. Nelson acknowledges Dr. Charles Ying for directing pulsed laser deposition techniques. Z. S., G. P., A. C. L., and R. W. B. acknowledge National Science Foundation (NSF) grant ECS-0355206, and L. N. acknowledges NSF grant ECCS-0651079 for financial support.

References

1. R. H. Ritchie, Phys. Rev. **106**, 874 (1957).
2. J. Homola, S. S. Yee, and G. Gauglitz, Sens. Actuators B **54**, 3 (1999).
3. M. Moskovits, Rev. Mod. Phys. **57**, 783 (1985).
4. W. L. Barnes, A. Dereux, and T. W. Ebbesen, Nature **424**, 824 (2003).
5. M. Danckwerts and L. Novotny, Phys. Rev. Lett. **98**, 026104 (2007).
6. S. Palomba and L. Novotny, Phys. Rev. Lett. **101**, 056802 (2008).
7. K. MacDonald, A. Krasavin, and N. Zheludev, Opt. Commun. **278**, 207 (2007).
8. J. B. Pendry, L. Martin-Moreno, and F. J. Garcia-Vidal, Science **305**, 847 (2004).
9. A. V. Krasavin, K. F. MacDonald, A. S. Schwanecke, and N. I. Zheludev, Appl. Phys. Lett. **89**, 031118 (2006).
10. T. Kume, T. Amano, S. Hayashi, and K. Yamamoto, Thin Solid Films **264**, 115 (1995).
11. K. Seal, M. A. Nelson, Z. C. Ying, D. A. Genov, A. K. Sarychev, and V. M. Shalaev, Phys. Rev. B **67**, 035318 (2003).
12. D. A. G. Bruggeman, Ann. Phys. (Leipzig) **24**, 636 (1935).
13. R. Landauer, J. Appl. Phys. **23**, 779 (1952).
14. X. C. Zeng, D. J. Bergman, P. M. Hui, and D. Stroud, Phys. Rev. B **38**, 10970 (1988).
15. P. B. Johnson and R. W. Christy, Phys. Rev. B **6**, 4370 (1972).
16. D. J. Bergman and D. Stroud, Solid State Phys. **46**, 147 (1992).
17. D. Stroud, Superlattices Microstruct. **23**, 567 (1998).
18. A. K. Sarychev, R. C. McPhedran, and V. M. Shalaev, Phys. Rev. B **62**, 8531 (2000).
19. R. Lazzari and I. Simonsen, Thin Solid Films **419**, 124 (2002).
20. J. J. Burke, G. I. Stegeman, and T. Tamir, Phys. Rev. B **33**, 5186 (1986).